CHAPTER-1

General Introduction

1. Introduction

1.1. Photoredox reaction

Visible-light photoredox catalysis, a fast-growing field, uses light-absorbing catalysts to generate reactive intermediates via electron transfer, enabling diverse organic transformations under mild conditions.[1-16] This approach enhances existing reactions and unlocks new chemical reactivity while reducing environmental impact.

Photoredox catalysis in organic synthesis began over 4 decades ago, with early work by Kellogg (1978) showing that $[Ru(bpy)_3]^{2+}$ accelerates sulfonium ion reduction via photomediated pathways.[17,18] Follow-up studies by Fukuzumi, Tanaka, and Pac expanded its use to reduce various substrates like olefins, ketones, and halides.[19-24] Deronzier later applied $[Ru(bpy)_3]^{2+}$ in a photochemical Pschorr reaction (1984), marking a milestone in synthetic applications.[25-27] Despite advancements, most reactions still rely on a limited set of photocatalysts. Landmark contributions include Okada's use of N-(acyloxy)phthalimides for alkyl radical generation and Yoon's [2+2] enone cycloaddition (2008).[28-30] However, the field gained widespread attention when MacMillan's group combined photoredox catalysis with organocatalysis for asymmetric aldehyde alkylation, marking a turning point in visible-light-driven synthesis.[31]

Similarly, organic dyes such as Eosin Y, 9,10-dicyanoanthracene, triphenylpyrylium, acridinium dyes, Rose Bengal, phenoxazines, and Rhodamine G have also proven to be effective photoredox catalysts, facilitating a wide range of bond-forming reactions in organic synthesis.[32-35] However, both transition metal-based and organic dye-based photoredox catalysts face several limitations, including difficulties in catalyst recovery and reuse, metal toxicity and high costs, susceptibility to photobleaching and degradation, short excited-state

lifetimes, sensitivity to reaction conditions, narrow light absorption ranges, challenges in scaling up processes, and the generation of chemical waste.[36-38]

In recent years, inorganic semiconductors (TiO_2, ZnO, MoS_2, WO_3, CdS, $BiVO_4$, etc.) have gained significant attention for solar energy applications, including energy conversion and organic transformations like molecular oxygen activation, hydrogen production, and CO_2 reduction to hydrocarbons.[39-42] However, their practical application is limited by several drawbacks, including a wide bandgap that restricts light absorption primarily to the ultraviolet (UV) region, poor utilization of visible light, rapid charge recombination, low redox potential, photocorrosion under prolonged irradiation, catalytic instability, low surface area, and reduced quantum yield, all of which hinder long-term catalytic performance and overall efficiency.[43-44] As a result, researchers have developed various techniques to create stable and ideal semiconductor photocatalysts that meet all the conditions mentioned above.

Recently, halide perovskites have emerged as promising photocatalysts due to their tunable band gaps and favourable conduction and valence band positions (CBM and VBM).[45-48] They offer several key advantages, including strong visible-light absorption, high photoluminescence quantum yield (PLQY), excellent charge carrier mobility, low charge recombination, and a large extinction coefficient, making them highly suitable for photoredox reactions and energy conversion.[49-50] The tunable bandgap allows precise adjustment of optical properties to optimize photocatalytic performance. Additionally, the soft lattice structure of $CsPbBr_3$ QDs facilitates integration with other semiconductor materials (TiO_2, ZnO, MoS_2, WO_3, CdS, $BiVO_4$, etc.) to form heterojunctions, improving charge separation and broadening light absorption.[51] These attributes have positioned metal halide perovskites as a highly versatile material for applications in pollutant degradation, water splitting, CO_2 reduction, and

organic transformations.[52]

1.2. Photocatalysis with semiconductor

Semiconductor-based photocatalysts have a valence band (VB) composed of the highest occupied molecular orbitals and a conduction band (CB) composed of the lowest unoccupied molecular orbitals.[53] The energy difference between the VB and CB is known as the bandgap energy (E_g).[54-55] When the photocatalyst absorbs light with energy equal to or greater than E_g, electrons are excited from the VB to the CB, leaving holes in the VB **(Figure 1.1)**. This creates an electron-hole pair, initiating the photocatalytic process.[56] The return of these excited electrons to their ground state without participating in chemical reactions is known as a photophysical process.[57] Photocatalysis follows four key steps: (i) Light absorption, generating electron-hole pairs, (ii) Separation of the excited electrons and holes, (iii) Migration of charge carriers to the catalyst surface, (iv) Surface redox reactions, driven by the electrons and holes **(Figure 1.1)**.[58-60] During the third step, many charge carriers recombine, either in the bulk or

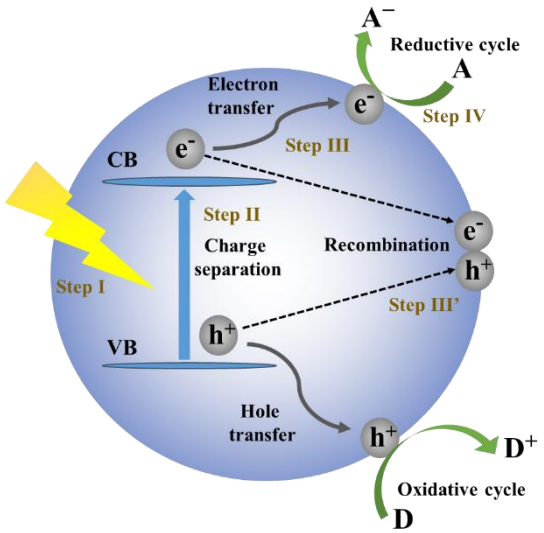

Figure 1.1. Steps in the photocatalytic reaction process. (i) Light absorption generates electron–hole pairs. (ii) Excited charge carriers (electrons and holes) separate. (iii) Electrons and holes migrate to the photocatalyst surface. (iii) Competing process: charge recombination. (iv) Surface charges drive redox reactions (A: Electron acceptor, D: Electron donor)

at the surface of the photocatalyst. This recombination releases energy either as heat (nonradiative) or light (radiative), reducing overall efficiency. Only the long-lived charge carriers that reach the surface can effectively participate in redox reactions. The nature of these reactions depends on the redox potential of the photogenerated charges (VB and CB) and the donor or acceptor characteristics of surface-adsorbed species **(Figure 1.1)**.[61]

1.3. Thermodynamic feasibility of photoredox generation of reactive oxygen species

The efficiency of photocatalysts is primarily governed by the dynamics of charge carriers at each stage of the photocatalytic process. For high-performance photocatalysis, materials should exhibit strong light absorption, efficient separation of photogenerated electron–hole pairs, high charge carrier mobility, minimal recombination losses and suitable bandgap **(Figure 1.2)**.[62-65]. Specifically, the conduction band minimum (CBM) must lie at a more negative potential than the target reduction reaction, while the valence band maximum (VBM) should be more positive than the oxidation potential **(Figure 1.2)**.[69,70] For an ideal photocatalyst, the optimal bandgap for driving photocatalytic organic reactions generally lies

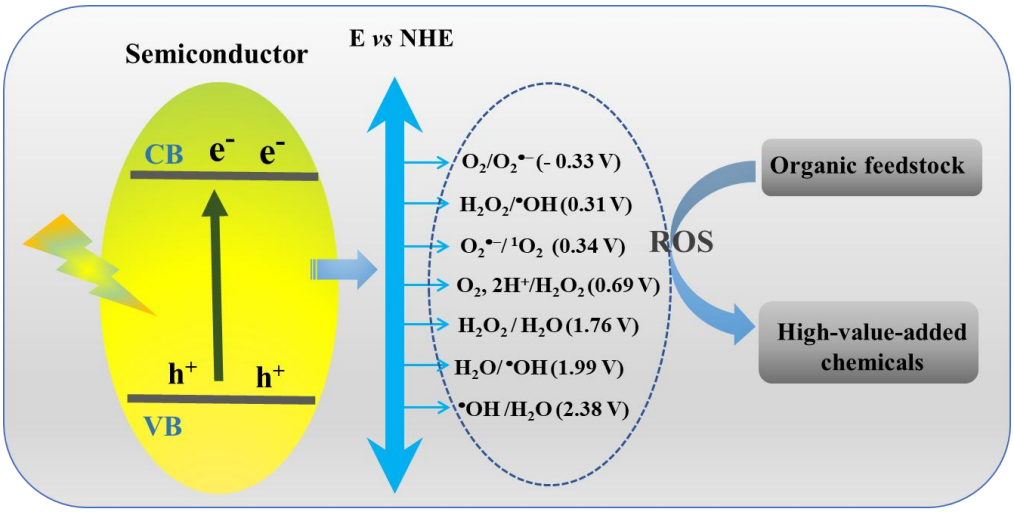

Figure 1.2. Reactive oxygen species (ROS) are produced during the photocatalytic reduction of oxygen and water oxidation. Left: redox potentials of various ROS. These species possess suitable oxidative power and play a key role in the selective oxidation of organic feedstocks into high-value-added chemicals.

between 1.8 and 2.8 eV.[71,72]

In this context, reactive oxygen species (ROS) are central to driving organic transformations. Upon light excitation, photogenerated charge carriers may either recombine or migrate to the semiconductor surface, where they engage in redox reactions **(Figure 1a)**. The electrons act as reducing agents and the holes as oxidizing agents, enabling the activation of oxygen or water molecules to yield ROS, including superoxide ($O_2^{\bullet-}$), singlet oxygen ($^1O_2$), hydroxyl radicals ($^{\bullet}OH$), etc.

1.4. Current strategies to enhance charge transport and suppress charge recombination in photoredox reactions

One major limitation of photocatalysts in a photoredox reaction is the rapid charge carrier recombination.[73] An ideal photocatalyst should exhibit strong light absorption, efficient charge separation and transport, low recombination rates, and long carrier diffusion distances.[74] Among these factors, charge separation and transfer are especially critical for driving photocatalytic reactions. Since charge separation and recombination are competing processes that occur on the nanosecond timescale, achieving ultrafast charge transfer is crucial.[75]

In previous sections, we examined the fundamental mechanisms and challenges related to the use of semiconductors in photoredox reaction processes. To overcome these limitations, a range of strategies has been developed to enhance charge separation and transfer, while simultaneously improving photocatalytic activity and selectivity.[76,77] For instance, including composition tuning (via doping, bandgap engineering, and morphology control), surface modification, cocatalyst integration, and the construction of heterojunction photocatalysts.[78,79]

1.4.1. Roles of cocatalysts in photocatalytic reactions

The cocatalysts in photocatalytic systems boost semiconductor activity and stability by

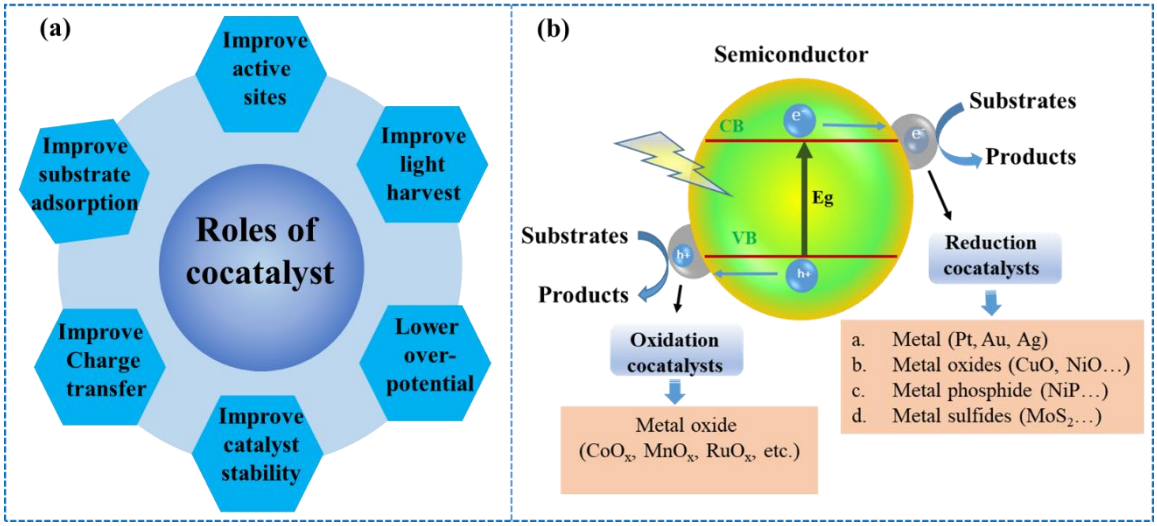

Figure 1.3. (a) Roles of cocatalysts in photocatalytic reactions. (b) Schematic representation of different types of cocatalysts involved in photocatalytic reduction and oxidation processes.

suppressing charge recombination, enhancing charge separation via heterojunctions, offering active catalytic sites, improving light absorption (e.g., via plasmonic metals or graphene), promoting reactant adsorption through high surface area and π–π interactions, and reducing photocorrosion to protect unstable materials **(Figure 1.3a)**.[80]

1.4.2. Categories of cocatalysts

Cocatalysts can be classified by the type of charge carriers they trap and their function in photocatalytic processes: reduction cocatalysts, which trap photogenerated electrons, and oxidation cocatalysts, which trap photogenerated holes (**Figure 1.3b**). Typically, materials such as noble and non-noble metals, certain metal oxides (e.g., CuO, NiO), metal hydroxides, metal sulfides, metal phosphides (e.g., Co_2P, Ni_2P), carbonaceous materials and transition metal complex act as reduction cocatalysts, facilitating photocatalytic hydrogen evolution, CO_2 reduction, molecular oxygen activation and help in hydrogen atom transfer process.[81] In contrast, some transition metal oxides (e.g., MnO_x, CoO_x, Fe_2O_2) and phosphides (e.g., Co–Pi) are primarily used as oxidation cocatalysts in photocatalytic oxygen evolution and pollutant

degradation reactions **(Figure 1.3b)**.[82,83]

1.4.3. Construction of heterojunction-based photocatalysts

The single-component semiconductor photocatalysts often suffer from limited efficiency.[84] In this respect, Semiconductor-based heterostructure photocatalysts can effectively address the aforementioned challenges, including charge recombination, limited charge carrier mobility, and insufficient photoredox potentials.[85] Semiconductor-based heterostructures show optimal optical properties, controllable band gaps, and modulated optoelectronic properties, offering applications in light-emitting diodes, solar cells, photocatalytic energy conversion processes, and organic transformations.[86] The heterojunction formation effectively separates photogenerated electrons and holes while combining the benefits of each component. Among these, Z-scheme heterojunctions, composed of oxidation and reduction photocatalysts, are the most promising because of the advantages like: i) suppression of charge recombination, ii) availability of reducing electrons and oxidizing holes, iii) improved light absorption, iv) tuning of the lifetime of the charge carriers and v) Accelerate reaction kinetics.[87]

1.4.4. Type-I, Type-II, Type-III, Z-Scheme, and S-Scheme heterojunctions

A heterojunction forms when two semiconductors with different band energy levels are brought into contact. Based on their band alignment, heterojunctions are generally classified into three types: type I (straddling), type II (staggered), and type III (broken gap). In a typical type-I heterojunction, both the CB and VB of one semiconductor lie within the band edges of the other (**Figure 1.4a**). Under light irradiation, charge carriers tend to accumulate in one semiconductor, leading to poor electron–hole separation and reduced redox capability due to limited redox potential.[88]

In contrast, type-II (staggered) heterojunctions enable efficient charge separation, as electrons and holes are spatially separated into different semiconductors. This occurs when the CB and

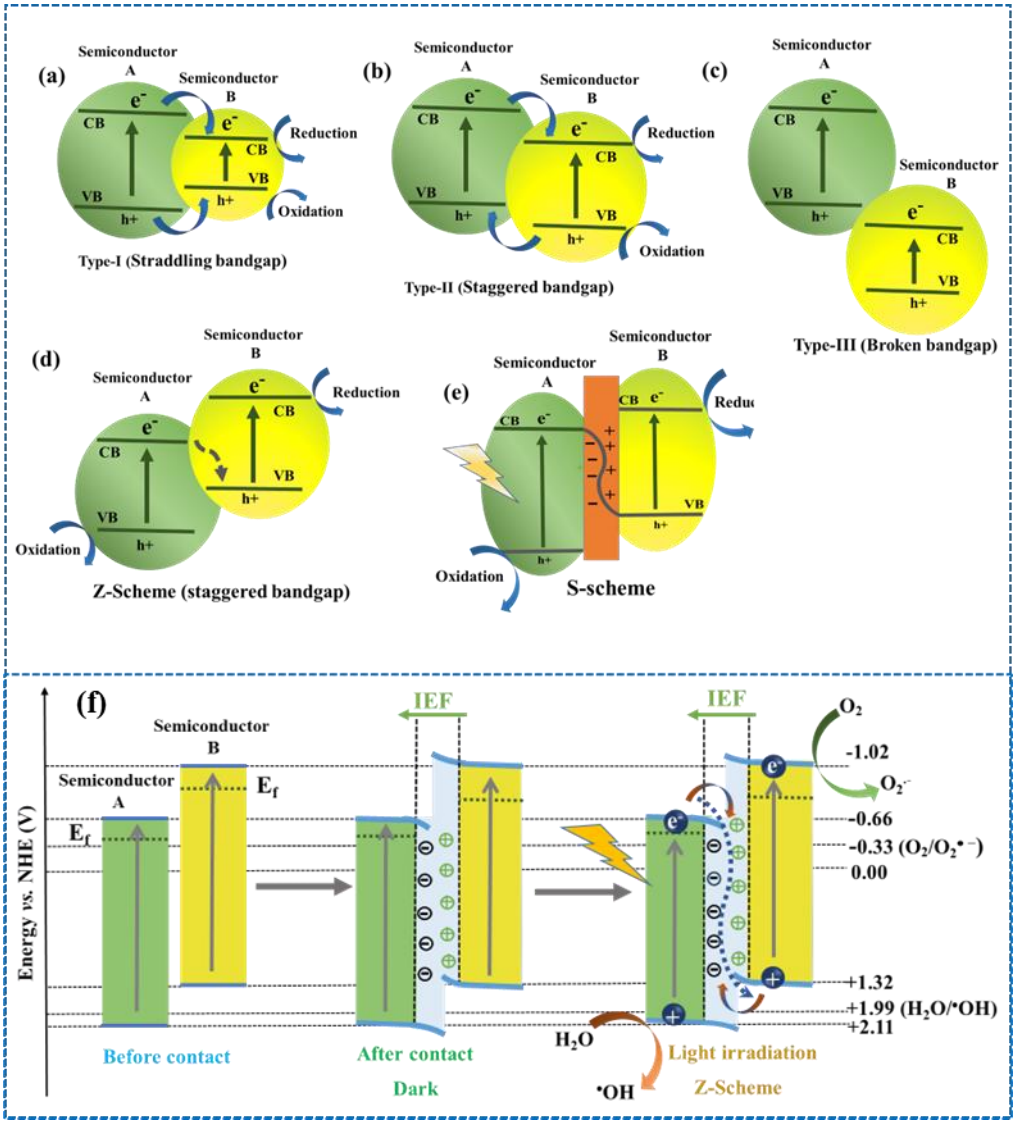

Figure 1.4. Energy band configurations of various heterojunction photocatalysts include: (a) Type-I (straddling gap), (b) Type-II (staggered gap), (c) Type-III (broken gap), and (d) Z-scheme systems, (e) S-scheme system, (f) Illustration of charge separation dynamics in a Z-scheme heterojunction showing: A) the individual semiconductor energy levels before physical contact, B) band alignment upon contact in the absence of light, and C) charge transfer behavior under light irradiation as the system reaches equilibrium.

VB of one semiconductor are both at higher energy levels than the other (**Figure 1.4b**), facilitating charge migration and enhancing photocatalytic activity.[89]

As a result, this type is generally unsuitable for photocatalysis. Among conventional heterojunctions, type-II remains the most favorable for enhancing photocatalytic activity due

to its ability to spatially separate charge carriers. Interfacial charge transfer influences band bending and alignment, shaping the heterojunction type. Type-II heterojunctions suffer from energy loss as high-energy carriers transfer across the interface, limiting photovoltage and redox potential, especially for reactions with $\Delta G > 2$ eV.[90]

In contrast, Z-scheme heterojunctions enable selective recombination of low-energy carriers while preserving high-energy electrons and holes for redox reactions. This design supports high-ΔG photocatalysis and enhances spatial charge separation and internal potential (**Figure 1.4d**). An emerging heterojunction design is the S-scheme (**Figure 1.4e**), which resembles a type-II staggered band structure but features a distinct charge-transfer mechanism. Unlike type-II systems, S-scheme heterojunctions retain high-energy charge carriers, electrons in the CB of the reduction photocatalyst and holes in the VB of the oxidation photocatalyst, while low-energy carriers recombine at the interface, generating a strong redox potential.[91]

When two semiconductors with different work functions are brought together, electrons flow from the one with the lower work function (semiconductor I) to the higher (semiconductor II), forming an internal electric field. Fermi level alignment induces band bending, driving electrons from semiconductor II and holes from semiconductor I to recombine at the interface via Coulombic attraction. As a result, only the high-energy carriers in semiconductor I (CB) and semiconductor II (VB) remain active for photocatalytic reactions (**Figure 1.4f**).[92]

1.5. Metal halide perovskite photocatalyst

Metal halide perovskites (MHPs) were first identified in 1893, but their potential was not fully recognized until the late 20th century.[93] Interest in these materials began to grow in the 1990s, primarily due to their promising optical and electronic characteristics, which made them suitable for applications in transistors and light-emitting devices.[94] A major breakthrough

occurred in 2012 when MHPs were explored as light-absorbing components in dye-sensitized solar cells. Researchers soon discovered that, beyond enhancing light absorption, these materials also possessed excellent charge transport capabilities. This revelation spurred rapid advancements in perovskite-based photovoltaics, leading to single-junction devices achieving power conversion efficiencies exceeding 23% within a short timeframe.[95]

Interestingly, metal halide perovskites demonstrated dual functionality, not only efficiently separating charge carriers to generate electricity but also effectively recombining them to emit light. Their low rates of nonradiative recombination and superior color purity positioned them as strong candidates for optoelectronic applications such as light-emitting diodes (LEDs) and lasers.[96]

However, bulk perovskite materials face limitations in terms of photoluminescence quantum yield (PLQY). Two primary challenges contribute to this: (i) the presence of mobile ionic defects, which form easily and interfere with radiative processes, and (ii) the inherently low exciton binding energy, which reduces the likelihood of electron-hole recombination through light emission.[97] These issues are evident in the inconsistent photoluminescence observed across different crystalline grains, with grain boundaries typically showing weak emission and increased nonradiative losses.

To overcome these drawbacks, researchers have shifted focus to perovskite nanocrystals (NCs). These nanoscale structures not only improve PLQY but also enable emission tunability through quantum confinement effects, offering enhanced performance for next-generation optoelectronic devices.

1.5.1. Application of MHP photocatalyst

MHPs excel at driving redox reactions under mild conditions with efficient charge separation,

enabling effective electron-hole generation and transfer. These properties support a wide range of applications, including organic transformations, LEDs, transistors, CO_2 reduction, water splitting, pollutant degradation, and oxygen activation for ROS generation. In $CsPbBr_3$, valence band is mostly Pb 6p orbital and conduction band is characterized by hybridized Br 4p and Pb 6s orbitals, ensures strong light absorption and superior optoelectronic performance compared to conventional photocatalysts like TiO_2 and ZnO.[98]

1.6. Structural features of MHP

MHPs are ionic compounds typically represented by the formula ABX_3, where **A** is a monovalent cation, such as methylammonium (MA^+: $CH_3NH_3^+$), formamidinium (FA^+: $CH(NH_2)_2^+$), or cesium (Cs^+); **B** is a divalent metal cation like Pb^{2+}, Sn^{2+}, or Cu^{2+}; and **X** is a

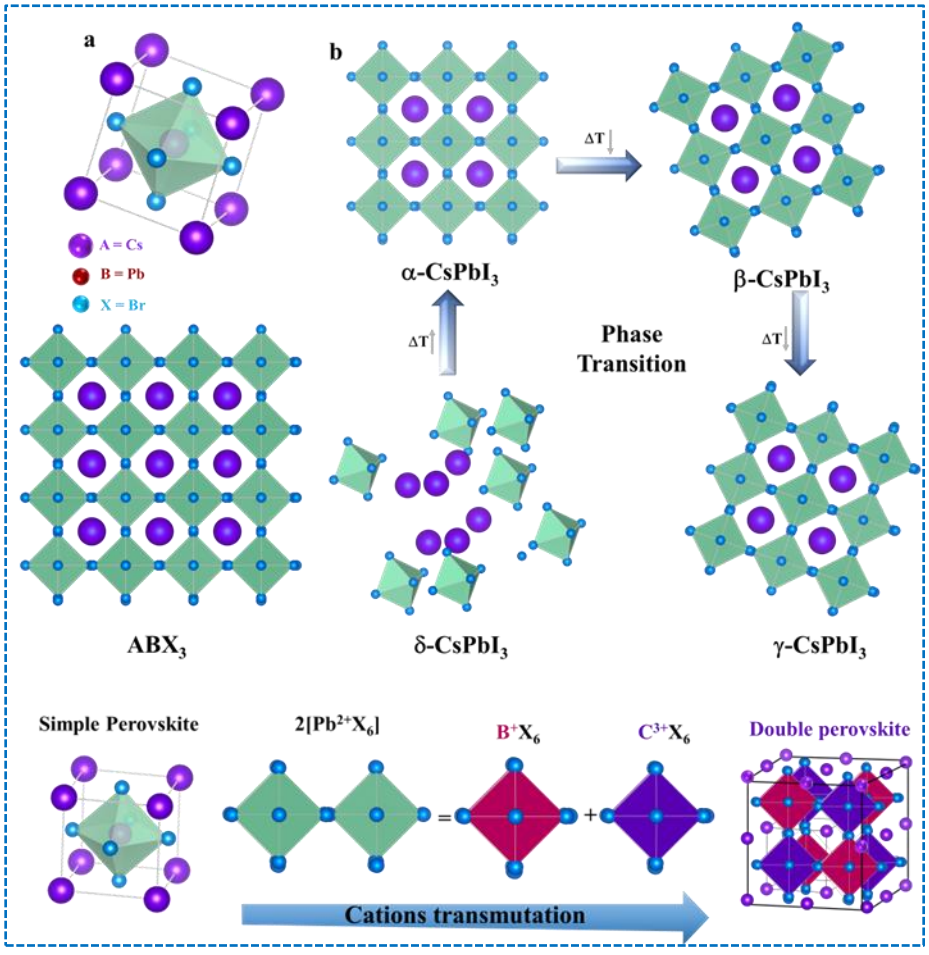

Figure 1.5. Structure, phase transformation, and cation transmutation in double perovskite.

halide anion (Cl^-, Br^-, I^-). Within this structure, the B-site cation is octahedrally coordinated by six halide ions to form $[BX_6]^{4-}$ units, which are embedded in a lattice stabilized by surrounding A-site cations **(Figure 1.5)**. Based on their elemental composition, these materials are categorized into organic–inorganic hybrid perovskites and fully inorganic perovskites.[99] To evaluate the geometric and structural stability of these perovskites, **Goldschmidt's tolerance factor** is commonly used in the formula. $\tau = \frac{r_A + r_B}{\sqrt{(r_B + r_X)}}$ This factor, calculated using the ionic radii of the A, B, and X ions (denoted as r_a, r_b, and r_x), provides insight into the feasibility of forming a stable 3D perovskite lattice.[100] A tolerance factor (**t**) between **0.8 and 1.0** generally indicates favorable structural conditions for a stable 3D perovskite framework and double perovskites **(Figure 1.5)**. If the A-site cation is too large and causes **t > 1**, the material often adopts a lower-dimensional configuration, such as two-dimensional perovskites (e.g., A_2PbI_4). Conversely, when **t < 0.8**, alternative structures like oxide perovskites (ABO_3) are more likely to form due to geometric instability.

1.7. Optical properties of MHP quantum dots (QDs)

Perovskite NCs, first synthesized in 2014, have since seen rapid research growth. Organic capping ligands enable nanoscale crystal growth and surface defect passivation, similar to traditional NCs. Their size and shape, bulk-like or as nanoplatelets, nanosheets, nanowires, or QDs, can be finely tuned, influencing optical emission, charge transport, and photoredox properties. Composition and structure can be modified during or after synthesis via ion exchange or exfoliation. Recent advances have achieved tunable visible-range emission and near-100% quantum yields (QY).[101] However, optical property studies lag, with photoluminescence quantum yields (PLQY) varying by synthesis, stoichiometry, and surface chemistry, factors still not fully understood.

1.8. MHP QDs for photoredox reactions

Over recent decades, research on low-dimensional semiconductors has led to quantum dots (QDs), nanometer-sized "artificial atoms" with quantum confinement and tunable properties. Initially based on group IV and III–V materials, QDs now include II–VI, I–III–VI compounds, dichalcogenides, and carbon-based types.[102] Their size-dependent bandgap, strong photoluminescence, and stability support applications from electronics to imaging. Recently, QDs have emerged as efficient photocatalysts due to high light absorption, charge separation, and surface tunability, enabling solar water splitting, CO_2 reduction, and pollutant degradation. Though traditional QDs like CdS, CdSe, and carbon dots aid photoredox reactions, they suffer from poor charge dynamics and limited active sites. Halide perovskite QDs (e.g., $CsPbBr_3$) now offer improved light absorption and electronic tunability for advanced photocatalysis. Semiconductor photocatalysts with tunable band gaps enable control over light response and redox reactions. Traditional materials like TiO_2, ZnO, CdS, and CdSe dominate the field but suffer from complex synthesis, high costs, poor stability, fast charge recombination, and limited visible-light use.

In this respect, $CsPbBr_3$ QDs have emerged as efficient, versatile photocatalysts with unique structural and electronic properties such as tunable band gaps, strong light absorption, high charge mobility, thermal stability, and long carrier diffusion, making them ideal for visible-light-driven reactions. Recently, various groups explored $CsPbBr_3$ for different types of photoredox organic transformations **(Figure 1.6).**[87,90-95,103-111]

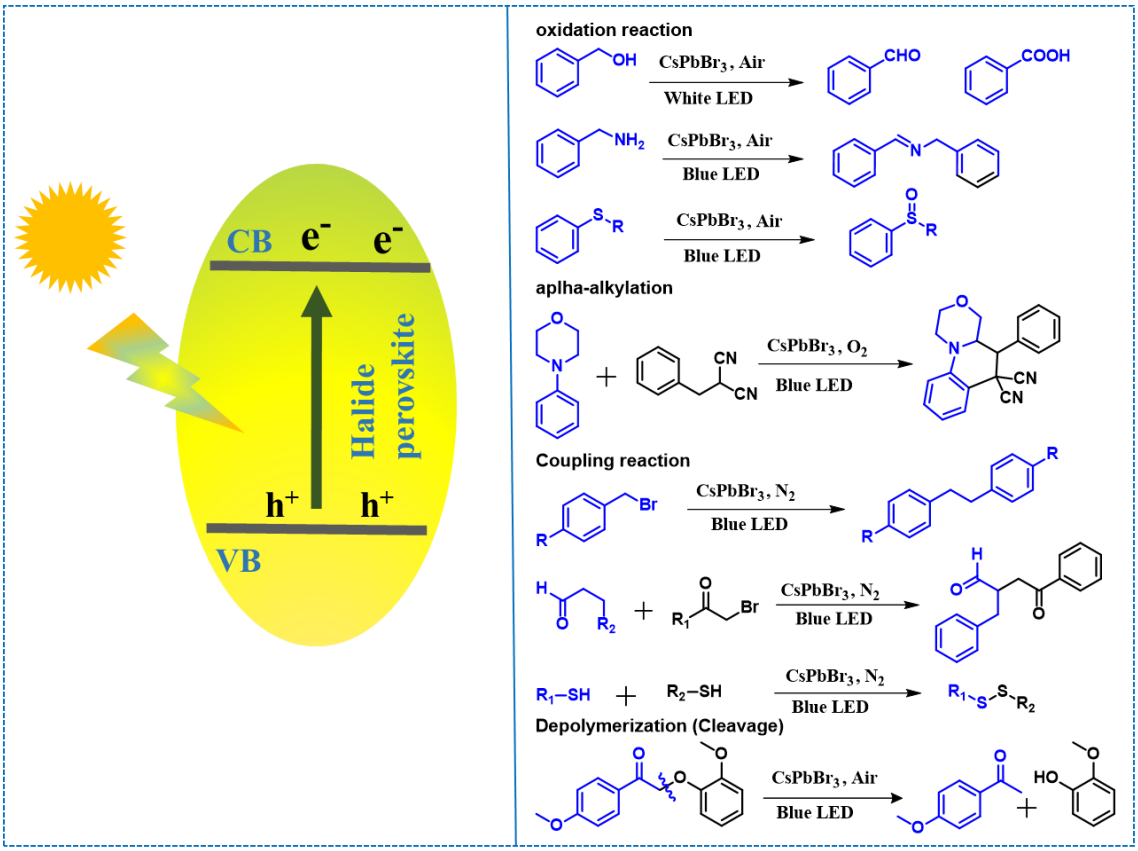

Figure 1.6. Different types of organic photoredox reactions carried out using halide perovskites.[90-95,103-111]

1.9. Band structure of $CsPbBr_3$ QDs

The MHPs have emerged as promising photocatalysts due to their unique (photo)physical properties. Compared to more traditional photocatalysts, MHPs exhibit relatively narrow bandgap energies, enabling the absorption of lower-energy solar photons **(Figure 1.7)**.[112] Based on reaction thermodynamics, effective photocatalysis requires a suitable alignment between the electronic band structure of the semiconductor and the redox potential of the target reactions.

The redox potentials of typical photocatalytic half-reactions, such as water splitting, CO_2 reduction, reactive oxygen species (ROS) generation, aerobic organic transformations, and dye degradation, alongside the relative positions of CB and VB of various MHPs, are described **(see Figure 1.2 and Figure 1.7)**.[113] The comparison reveals the excellent reduction ability of

MHPs, as their CB positions are typically negative enough to drive reactions like H_2 generation, CO_2 reduction, and superoxide radical formation.[114] Additionally, certain MHPs, specifically Cl-based materials and all-inorganic $CsPbBr_3$, possess relatively positive VBM, theoretically allowing for water oxidation.[115] However, MHPs are generally unsuitable for hydroxyl radical formation, which is essential for dye degradation, because the required potential lies above their VBM. Despite this limitation, MHPs meet several key criteria for efficient photocatalysis (**Figure 1.7**).[109-111]

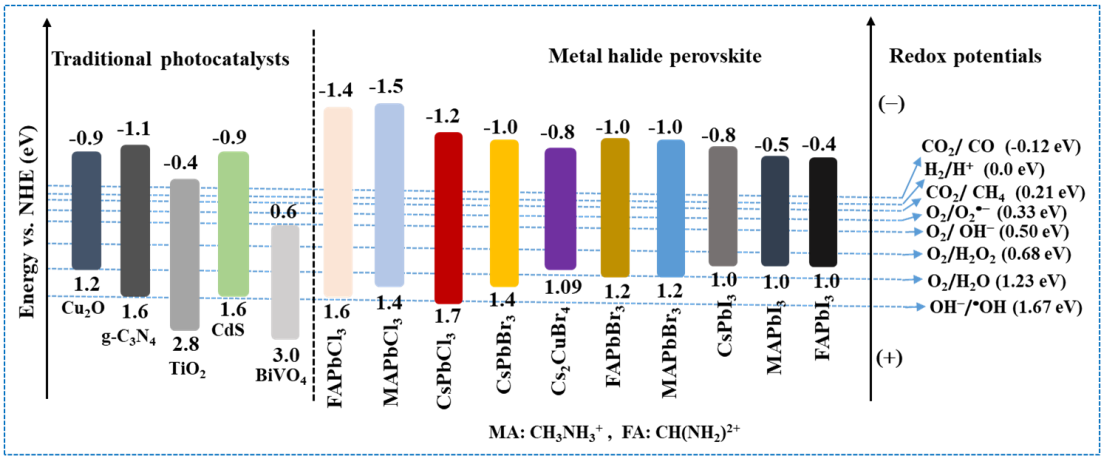

Figure 1.7. Band edge positions of conventional photocatalysts and different MHPs relative to the reversible hydrogen electrode (NHE). For comparison, the redox potential of some common half-reactions is also presented.

1.10. Stability of metal halide perovskite

The structural and optoelectronic properties of MHPs are highly sensitive to external stimuli, undergoing significant changes in response to phase transitions, thermal stress, exposure to ambient air (particularly oxygen and moisture), and ultraviolet (UV) illumination.[116] A key contributor to this instability is the ionic nature of MHP crystals; the electrostatic interactions between charged components make their surfaces especially susceptible to structural modification upon contact with polar additives.[117]

This intrinsic sensitivity has consequently restricted the range of photocatalytic reactions

for which MHPs have been effectively employed. When exposed to polar environments, MHPs tend to decompose rapidly, yielding lead halide (PbX_2, where X = I, Br, or Cl) precipitates, organic (MA^+, FA^+) or inorganic (Cs^+) cations, and halide anions. In hybrid organic–inorganic MHPs, moisture instability is further exacerbated by the volatile and hygroscopic nature of the amine-based organic cations (MA^+ and FA^+).[118,119] Water interacts with the MHP crystal through hydrogen bonding, leading to surface hydration and the formation of a polycrystalline, non-perovskite structural coating along with grain boundary development.[120]

1.11. Characterization techniques for charge behaviour induced by cocatalysts

Charge carrier dynamics are critical to photocatalytic performance. As noted, a key role of cocatalysts is to trap photogenerated charge carriers at the interface and suppress their recombination. To investigate this function, various characterization techniques are employed to evaluate charge separation in the interfacial region during photocatalysis. These include surface photovoltage microscopy, transient absorption spectroscopy, photocurrent, EIS measurements, and steady-state or time-resolved photoluminescence (PL) spectroscopy.

1.12. Role of reactive oxygen species (ROS) in photocatalysis

Photocatalysis involves light-induced excitation of electrons from the VB to the CB of a semiconductor, generating electron–hole pairs. These charge carriers can recombine or migrate to the catalyst surface to drive redox reactions.[113] In aqueous, aerobic environments, photogenerated electrons and holes react with O_2, H_2O, or surface OH groups to produce ROS such as superoxide radical ($^{\bullet}O_2^-$), hydrogen peroxide (H_2O_2), hydroxyl radical ($^{\bullet}OH$), and singlet oxygen ($^1O_2$), which initiate the radical reactions **(see Figure 1.2)**. These species, alongside holes, are key oxidants in photocatalytic degradation and organic synthesis.[115] •OH, in particular, drives nonselective oxidation to CO_2 and H_2O. Hence, controlling ROS

generation is critical for improving selectivity in photocatalytic reactions, with photocatalyst and solvent choice influencing ROS pathways and reactivity **(see Figure 1.2)**.[112]

1.13. Importance of amide, amine, and heterocyclic compounds

1.13.1. Importance of amides

Amide bonds are pivotal structural units in organic molecules and are particularly significant in organic synthesis and medicinal chemistry.[122-123] These bonds are essential to constitute the backbone of proteins and peptides and are integral to numerous bioactive compounds. Consequently, the development of efficient and practical strategies for amide bond formation remains a major focus for both academic and industrial researchers **(Figure 1.8)**.[124]

Recent progress in amide bond synthesis has introduced milder and more selective methods, which facilitate the construction of amide linkages under diverse reaction conditions. These advancements have greatly enhanced the preparation of peptides, which are vital in pharmaceutical development, chemical biology, and biotechnological applications.[125]

In parallel, photocatalytic approaches for synthesizing amides from aldehydes and amines have attracted considerable interest. Amides are not only the building blocks of peptides but also serve as key intermediates in producing materials such as polymers, agrochemicals, and pharmaceuticals. Conventional thermal condensation methods involving carboxylic acids and amines often require harsh conditions, limiting their applicability.[126] Similarly, classical transformations using activated acid derivatives, such as the Beckmann rearrangement, Schmidt reaction, and Staudinger ligation, can generate significant chemical waste, raising environmental concerns.[127]

To address these limitations, alternative photocatalytic methods are being explored as sustainable and efficient solutions. However, many existing homogeneous photocatalytic

systems still face challenges, including the use of expensive catalysts, reliance on non-oxygen oxidants, and poor compatibility with secondary amines. Simpler and more accessible photocatalysts, including phenazine salts, Rose Bengal, and aminoanthraquinone-based systems, have shown encouraging results. Additionally, heterogeneous photocatalysts such as Ag/*g*-C_3N_4, Ni/*g*-C_3N_4, Ag_2O/P-C_3N_4, TiO_2, and Fe_3O_4/PDA/CdS have been successfully applied for oxidative amidation of aldehydes and amines, offering more practical and reusable alternatives.[128,129]

1.13.2 Importance of Amines

Nitrogen-containing organic moieties, often referred to as "amines" or "amino groups," are crucial building blocks in various biologically active compounds and have significant applications across multiple fields of chemistry **(Figure 1.8)**.[130] Amines and their nitrogen containing derivatives are important in natural products, biologically active molecules, pharmaceuticals, and polymers as intermediates and key precursors.[131] The *N*-alkylation of amines with alcohols is superior to traditional methods (reduction amination, alkylation of ammonia/amines using alkyl halides, reduction of nitriles, etc.).[132] *N*-alkylation is a green synthesis method for organic amines, which includes mild conditions, readily available, cost-effective raw materials, and the exclusive generation of water as a byproduct. Generally, this reaction involves three steps: dehydrogenation of alcohols to form aldehydes, condensation of aldehydes with amines leading to imines, and hydrogenation of imines to the desired amines, which proceeds by the “transfer hydrogen” or “borrowing hydrogen” mechanism.[133-135]

The hydrogen atom transfer and borrowing hydrogen processes allow sustainable functionalization of amines using alcohols. The process is more advantageous as no external hydrogen source is required, and the parent alcohol acts as the hydrogen donor. Moreover, it

should be noted that various alcohols are readily accessible from renewable feedstocks, making this approach particularly well-suited for the valorization of biomass or biomass-derived building blocks.[135]

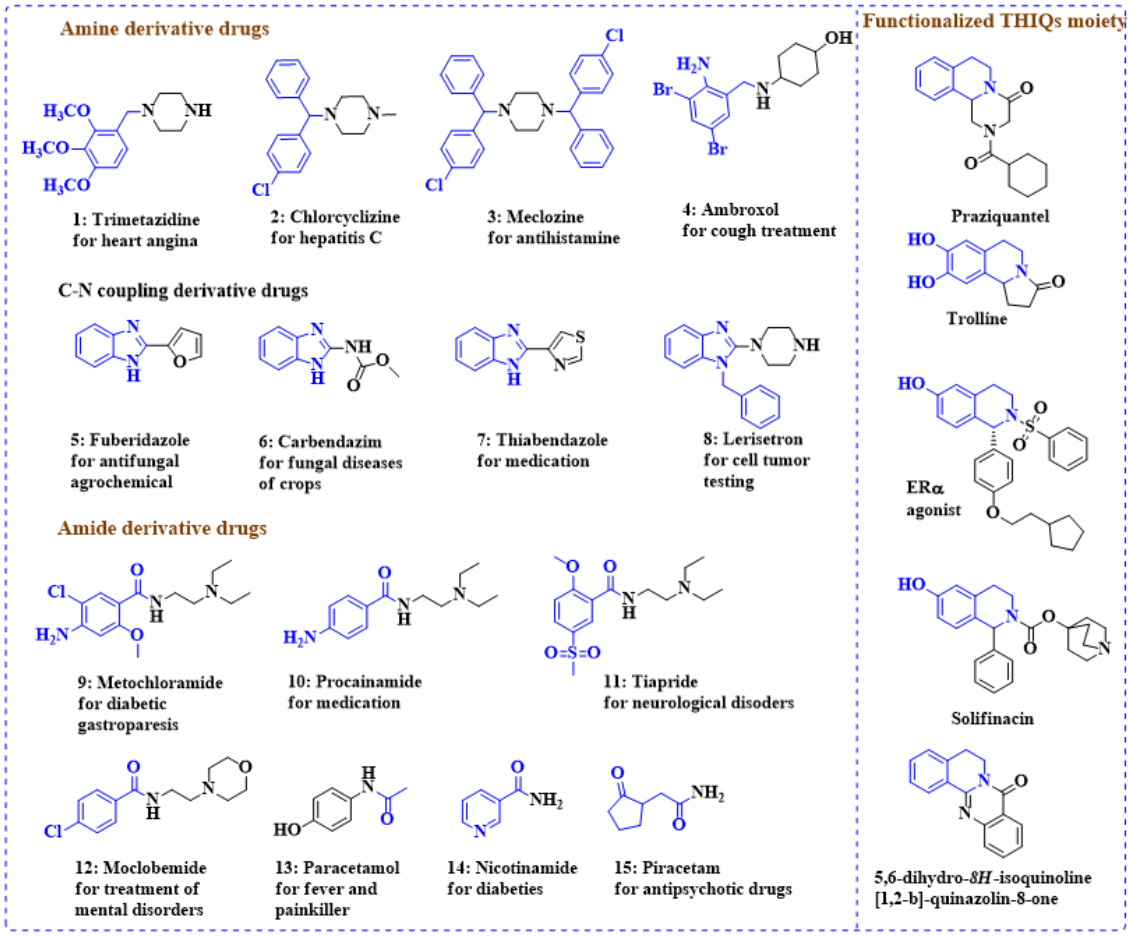

Figure 1.8. Examples of the different types of drugs with amine and amide moieties.

Previously, Beller, Balaraman, and Kempe groups explored homogeneous noble metal (Ru, Ir, etc.) complexes for the N-alkylation of amine.[136] However, these catalysts face low stability, the use of expensive ligands, and poor recyclability. In this respect, transition metal heterogeneous catalysts have shown notable advantages in terms of durability and recoverability. These catalysts also suffer from low activity, poor selectivity, and high reaction

temperature requirements.[137]

In this context, photoredox reactions using semiconductors provide an important platform. Recently, different photocatalysts have been successfully applied to organic transformation reactions, achieving selectivity and activity comparable to homogeneous catalysts.[138-140] Recently, Zhang group reported CdS for photocatalytic imine and amine synthesis with the help of formic acid and sodium formate as a hydrogen donor. Still, this method required an external hydrogen source.[141] Further, Li group demonstrated the Ni–Fe-MOF as a catalyst for the *N*-alkylation of amines with alcohols under visible light.[142] However, these approaches suffer from poor selectivity of amine formation, the requirement for external sources of hydrogen, and significant waste production.

1.13.3. Importance of isoquinoline compounds

1,2,3,4-tetrahydroisoquinoline (THIQ) and related N-heterocycles are key intermediates in the pharmaceutical and petrochemical industries, with applications in drugs, agrochemicals, fine chemicals, dyes, fragrances, and hydrogen-storage materials.[143-144] These compounds are typically obtained through the selective hydrogenation of isoquinolines. However, this transformation remains challenging due to catalyst poisoning, the high energy required to disrupt aromaticity, and competition between the benzene and pyridine rings during hydrogenation.[145] Traditional hydrogenation methods often require harsh conditions, including high hydrogen pressures (2.5−60 bar) and elevated temperatures (353−433 K). In contrast, transfer hydrogenation using safer sources like formic acid, alcohols, or ammonia borane enables milder conditions.[146,147] Visible-light-driven reactions offer high selectivity and sustainability. However, photocatalytic transfer hydrogenation of quinolines remains underexplored despite its promising potential for green chemical transformations.

Recent studies show THIQ semidehydrogenation to 3,4-dihydroisoquinoline (DHIQ) is challenging, with Wang and Bahnemann groups reporting isoquinoline (IQ) or mixed products using h-BCN and Rh/TiO_2, respectively.[148,149] Shi achieved selective DHIQ formation with $Zn_3In_2S_6$ and O_2, while Li used $MoS_2/ZnIn_2S_4$.[150,151] Here, we report a Z-scheme BiOBr NSs/$CsPbBr_3$ QDs heterojunction for efficient THIQ semidehydrogenation using O_2 as a green electron acceptor.

1.14. Objectives of the thesis

The primary objective of this thesis is to build upon insights from previous literature to investigate the optical properties of metal halide perovskite QDs and nanocrystals for selective photoredox organic transformations. Specifically, we investigated the design of halide perovskite photocatalysts and analysed their redox potentials, namely, the VB and CB positions, about key organic transformations such as oxidative amidation of alcohols and N-alkylation of anilines. We also examined the influence of metal complex cocatalysts on photogenerated charge dynamics and overall photoredox activity.

This thesis is organized into six chapters, each briefly described below (Figure 1.9). To further enhance catalytic performance, we studied charge separation processes by introducing heterojunctions with other photocatalysts. This strategy not only improved charge separation efficiency but also allowed control over electron transfer in reactions such as the semidehydrogenation of 1,2,3,4-tetrahydroisoquinoline to 3,4-dihydroisoquinoline.

Additionally, we synthesized a lead-free metal halide perovskite photocatalyst (Cs_2CuBr_4) for C–N bond formation under visible-light irradiation. We examined the effects of synthesis method variations on band structure modulation and charge dynamics. Reaction conditions were optimized to achieve high yields and selectivity. The photocatalyst showed excellent

stability and was effectively reused across multiple cycles without loss of activity.

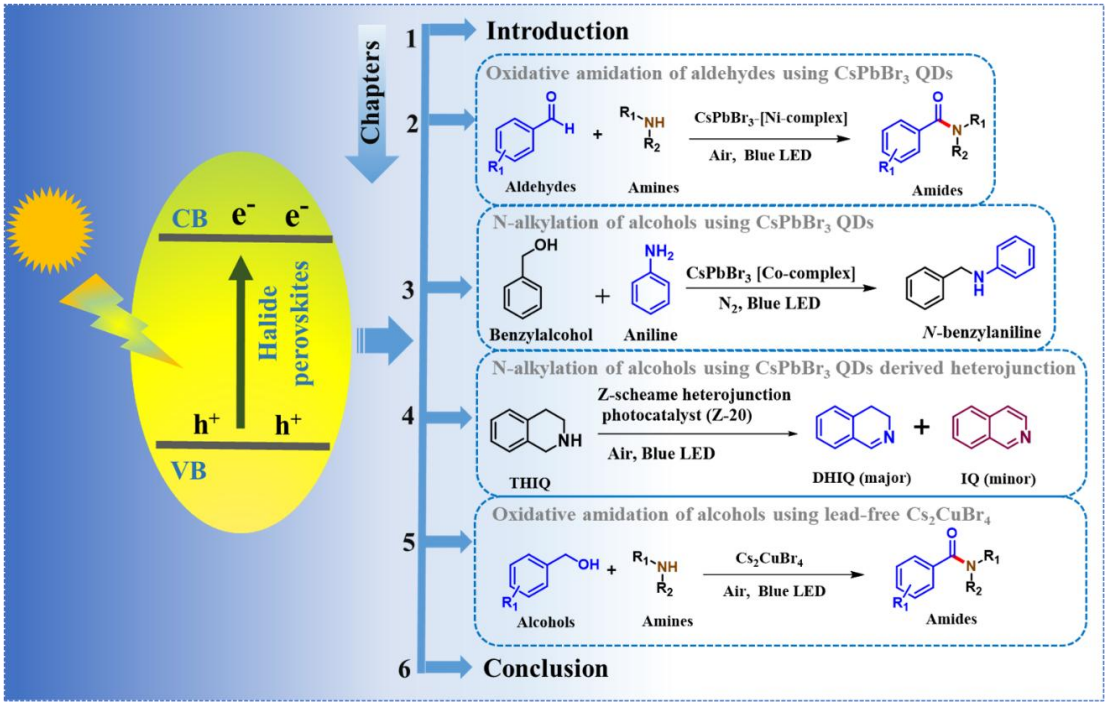

Figure 1.9. A diagram showing the chapter-wise specific objectives of the thesis.

Chapter 2: In the second chapter, $CsPbBr_3$ QDs were used as photocatalysts for C–N bond formation, with $Ni(dmgH)_2$ (dmgH = dimethyl glyoximato) serving as an effective cocatalyst to enhance amide synthesis. Optimal interaction between the QDs and 7 wt% $Ni(dmgH)_2$ improved charge transfer, reduced recombination, and increase the product yield up to 92%. Femtosecond transient absorption spectroscopy revealed cocatalyst-induced changes in QD trap-state dynamics. $Ni(dmgH)_2$ also activated molecular oxygen to generate superoxide radicals, driving the radical C–N coupling pathway. The catalyst remained active over four reuse cycles without loss of efficiency.

Chapter 3: In this chapter, we demonstrate the $CsPbBr_3$ QDs for photocatalytic N-alkylation of amines with alcohols, a cost-effective and efficient route using the borrowing hydrogen (BH) strategy. By tuning the LUMO energy of cobaloxime cocatalysts through modifications to the Co center's electronic environment, we achieved selective N-alkylation.

In this process, alcohols serve as both aldehyde precursors and hydrogen sources. The perovskite QDs, known for their low cost, ease of processing, air stability, and tunable band edges, offer promising potential in organic transformations. Furthermore, selectivity can be easily modulated by adjusting the cocatalyst's electronic structure.

Chapter 4: In this chapter, we developed the Z-scheme heterojunction of BiOBr nanosheets and $CsPbBr_3$ QDs for the selective semidehydrogenation of tetrahydroisoquinoline (THIQ) to dihydroisoquinoline (DHIQ). Charge separation is driven by interfacial electric fields, with electrons transferring from BiOBr's CB to $CsPbBr_3$'s VB. The negative CB of $CsPbBr_3$ activates the molecular oxygen (O_2), forming reactive oxygen species. Optimal loading of $CsPbBr_3$ on BiOBr (20 wt%, Z-20) achieved a 97% yield and controlled the two-electron process for selective semidehydrogenation of THIQ to DHIQ. Transient absorption studies revealed efficient exciton dynamics, contributing to enhanced catalytic performance.

Chapter 5: In the fifth chapter, we report the modulation of lead-free metal halide perovskite (Cs_2CuBr_4) band structures by tuning synthesis methods. Photocatalyst PC-1, synthesized via hot injection, features a more negative conduction band minima (CBM) than PC-2, synthesized at room temperature, enabling more efficient O_2 activation and radical-mediated alcohol dehydrogenation. PC-1 also exhibits a more positive valence band maxima (VBM), facilitating amine oxidation: enhanced charge separation and reduced recombination further boost photocatalytic performance. PC-1 achieved up to 98% yield in the oxidative amidation of alcohols and is recyclable for over five cycles.

1.15. References:

1. A. Noble, and D. W. C. MacMillan, *J. Am. Chem. Soc.,* 2014, **136**, 11602–11605.
2. Z. Zuo, and D. W. C. MacMillan, *J. Am. Chem. Soc.,* 2014, **136**, 5257–5260.
3. S. Ventre, F.R. Petronijevic, and D. W. C. MacMillan, J. Am. Chem. Soc., 2015, 137, 5654–5657.

4. L. Candish, M. Teders, and F. Glorius, *J. Am. Chem. Soc.,* 2017, **139,** 7440–7443.
5. M. Zlotorzynska and G. M. Sammis, *Org. Lett.* 2011, **13,** 6264–6267.
6. G. Pratsch, G. L. Lackner, and L. E. Overman, *J. Org. Chem.* 2015, **80,** 6025–6036.
7. D. Rackl, V. Kais, P. Kreitmeier, and O. Reiser, *J. Org. Chem.* 2014, **10,** 2157–2165.
8. E.E. Stache, A. B. Ertel, T. Rovis, and A. G. Doyle, *ACS Catal.* 2018, **8,** 11134–11139.
9. J. A. Rossi-Ashton, J. K. Clarke, W. P. Unsworth, and R. J. K. Taylor, *ACS Catal.,* 2020, **10,** 7250–7261.
10. J. Z. Wang, H. A. Sakai, and D. W. C. MacMillan, *Angew. Chem. Int. Ed.* 2022, **134,** 202207150.
11. F. J. R. Klauck, M. J. James, and F. Glorius, *Angew. Chem. Int. Ed.* 2017, **56**, 12336–12339.
12. M. A. Ashley and T. Rovis, *J. Am. Chem. Soc.* 2020, **142,** 18310–18316.
13. J. R. Dorsheimer, and T. Rovis, *J. Am. Chem. Soc.* 2023, **145,** 24367–24374.
14. A. D. Marchese, J. R. Dorsheimer, and T. Rovis, *Angew. Chem. Int. Ed.* 2024, **63,** 202317563.
15. J. R. Dorsheimer, M. A. Ashley, and T. Rovis, *J. Am. Chem. Soc.,* 2021, **143,** 19294–19299.
16. S. Dongbang and A. G. Doyle, *J. Am. Chem. Soc.,* 2022, **144,** 20067–20077.
17. D. M. Hedstrand, W. M. Kruizinga, and R. M. Kellogg, *Tetrahedron Lett.* 1978, **19,** 1255−1258.
18. T. J. van Bergen, D. M. Hedstrand, W. H. Kruizinga, and R. M. Kellogg, *J. Org. Chem.* 1979, **44**, 4953−4962.
19. K. Hironaka, S. Fukuzumi, and T. Tanaka, *J. Chem. Soc., Perkin Trans.* 2 1984, 1705−1709.
20. S. Fukuzumi, S. Koumitsu, K. Hironaka, and T. Tanaka, *J. Am. Chem. Soc.* 1987, **109,** 305−316.
21. S. Fukuzumi, S. Mochizuki, and T. Tanaka, *J. Phys. Chem.* 1990, **94,** 722−726.
22. C. Pac, M. Ihama, M. Yasuda, Y Miyauchi, and H. J. Sakurai, *Am. Chem. Soc.* 1981, **103**, 6495−6497.
23. O. Ishitani, M. Ihama, Y. Miyauchi, and C. Pac, *J. Chem. Soc., Perkin Trans. 1* 1985, 1527−1531.
24. O. Ishitani, S. Yanagida, S. Takamuku, and C. Pac, *J. Org. Chem.,* 1987, **52,** 2790−2796.
25. H. Cano-Yelo and A. Deronzier, *Tetrahedron Lett.* 1984, **25,** 5517−5520.
26. H. Cano-Yelo and A. Deronzier, *J. Chem. Soc., Perkin Trans. 2,* 1984, 1093−1098.
27. H. Cano-Yelo and A. Deronzier, *J. Photochem.,* 1987, **37**, 315−321.
28. K. Okada, K. Okamoto, M. Oda, *J. Am. Chem. Soc.* 1988, **110**, 8736−8738.
29. K. Okada, K. Okubo, N. Morita, and M. Oda, *Tetrahedron Lett.* 1992, **33**, 7377−7380.
30. M. A. Ischay, M. E. Anzovino, J. Du, T. P. Yoon, *J. Am. Chem. Soc.,* 2008, **130**, 12886−12887.

31. D. A. Nicewicz and D. W. C. MacMillan, *Science* 2008, **322**, 77–80.
32. D. P. Hari and B. König, *Chem. Commun*, 2014, **50**, 6688–6699.
33. N. A. Romero and D. A. Nicewicz, *Chem. Rev..,* 2016, **116,** 10075–10166.
34. E. Speckmeier, T. G. Fischer, and K. Zeitler, *J. Am. Chem. Soc.,* 2018, **140,** 15353–15365.
35. B. G. McCarthy, R.M. Pearson, C. H. Lim, S.M. Sartor, N. H. Damrauer, and G. M. Miyake, *J. Am. Chem. Soc.,* 2018, **140,** 5088–5101.
36. C.B. Larsen and O.S. Wenger, *Chem. Eur. J.* 2018, **24**, 2039–2058.
37. B.M. Hockin, C.F. Li, N. Robertson, and E. Zysman-Colman, *Catal. Sci. Technol*., 2019, **9,** 889–915.
38. O.S. Wenger, *J. Am. Chem. Soc.,* 2018, **140,** 13522–13533.
39. W. Wang, M. O. Tade, and Z. Shao, *Chem. Soc. Rev.* 2015, **44,** 5371−5408.
40. J. Gong, C. Li, and M. R. Wasielewski, *Chem. Soc. Rev.* 2019, **48,** 1862−1864.
41. S. Zhu, and D. Wang, *Adv. Energy Mater.,* 2017, **7**, 1700841.
42. J. K. Stolarczyk, S. Bhattacharyya, L. Polavarapu, and J. Feldmann, *ACS Catal.,* 2018, **8**, 3602−3635.
43. T. M. Brenner, D. A. Egger, L. Kronik, G. Hodes, and D. Cahen, *Nat. Rev. Mater.,* 2016, **1**, 15007.
44. J. Chen, C. Dong, H. Idriss, O. F. Mohammed, and O. M. Bakr, *Adv. Energy Mater.,* 2020, **10,** 1902433.
45. V. Armenise, S. Colella, F. Fracassi, and A. Listorti, *Nanomater* 2021, **11,** 433.
46. Y. Tang, C. H. Mak, G. Jia, K. C. Cheng, J. Kai, C. Hsieh, W. Meng, W. Niu, F. Li, H. Shen, X. Zhu, H. Chen, and H.Y. Hsu, *J. Mater. Chem. A* 2022, **10,** 12296−12316.
47. P. Chen, W. J. Ong, Z. Shi, X. Zhao, and N. Li, *Adv. Funct. Mater.* 2020, **30,** 1909667.
48. H. Huang, B. Pradhan, J. Hofkens, M. B. J. Roeffaers, and J. A. Steele, *ACS Energy Lett.* 2020, **5**, 1107−1123.
49. C. Han, X. Zhu, J. S. Martin, Y. Lin, S. Spears, and Y Yan, *ChemSusChem* 2020, **13,** 4005−4025.
50. J. Wang, Y. Shi, Y. Wang, and Z. Li, *ACS Energy Lett.* 2022, **7**, 2043−2059.
51. H. Huang, D. Verhaeghe, B. Weng, B. Ghosh, H. Zhang, J. Hofkens, J. A. Steele, M. B. J. Roeffaers, *Angew. Chem., Int. Ed.* 2022**, 61**, 202203261.
52. K. Ren, S. Yue, C. Li, Z. Fang, K. A.M. Gasem, J. Leszczynski, S. Qu, Z. Wang and M. Fan, *J. Mater. Chem. A* 2022, **10,** 407−429.
53. S. Chen, T. Takata, and K. Domen, *Nat. Rev. Mater.* 2017, **2**, 17050.
54. M. G. Kibria, F. A. Chowdhury, S. Zhao, B. Otaibi, M. L. Trudeau, H. Guo, and Z. Mi, *Nat. Commun*. 2015, **6**, 6797.
55. Q. Wang, T. Hisatomi, Q. Jia, H. Tokudome, M. Zhong, C. Wang, Z. Pan, T. Takata, M. Nakabayashi, N. Shibata, Y. Li, I. D. Sharp, A. Kudo, T. Yamada, and K. Domen, *Nat. Mater.* 2016, **15**, 611.
56. Y. Hikita, K. Nishio, L. C. Seitz, P. Chakthranont, T. Tachikawa, T. F. Jaramillo, and

H. Y. Hwang, *Adv. Energy Mater.* 2016, **6**, 1502154.
57. Y. Kuang, Q. Jia, G. Ma, T. Hisatomi, T. Minegishi, H. Nishiyama, M. Nakabayashi, N. Shibata, T. Yamada, A. Kudo, and K. Domen, *Nat. Energy* 2017, **2**, 16191.
58. J. Li and N. Wu, *Catal. Sci. Technol*. 2015, **5**, 1360.
59. T. Simon, M. Carlson, J. Stolarczyk, and J. Feldmann, *ACS Energy Lett.* 2016, **1**, 1137.
60. T. Gershon, B. Shin, N. Bojarczuk, M. Hopstaken, D. B. Mitzi, and S. Guha, *Adv. Energy Mater.* 2015**, 5**, 1400849.
61. Z. Liang, R. Shen, Y. H. Ng, P. Zhang, Q. Xiang, and X. Li, *J. Mater. Sci. Technol.* 2020, **56**, 89.
62. T. Hisatomi, J. Kubota, and K. Domen, *Chem. Soc. Rev.* 2014, **43**, 7520−7535.
63. H. Zhou, Y. Qu, T. Zeid, and X. Duan, *Energy Environ. Sci.* 2012, **5**, 6732−6743.
64. M. Ge, Q. Li, C. Cao, J. Huang, S. Li, S. Zhang, Z. Chen, K. Zhang, S. Deyab, and Y. Lai, *Adv. Sci.* 2017, **4**, 1600152.
65. J. Wen, J. Xie, X. Chen, and X. Li, *Appl. Surf. Sci.* 2017, **391**, 72−123.
66. R. He, S. Cao, P. Zhou, J. Yu, and J. Chin. *Catal.* 2014, **35**, 989−1007.
67. M. M. Lee, J. Teuscher, T. Miyasaka, T. N. Murakami, and H. J. Snaith, *Science* 2012, **338**, 643−647.
68. J. K. Stolarczyk, S. Bhattacharyya, L. Polavarapu, and J. Feldmann, *ACS Catal.* 2018, 8, 3602−3635.
69. J. S. Manser, J. A. Christians, and P. V. Kamat, *Chem. Rev.* 2016, **116**, 12956.
70. S. Chen, H. Yin, P. Liu, Y. Wang, and H. Zhao, *Adv. Mater.* 2023, **35,** 2203836.
71. A. Kojima, K. Teshima, Y. Shirai, and T. Miyasaka, *J. Am. Chem. Soc.* 2009, **131**, 6050.
72. A. Swarnkar, V. K. Ravi, and A. Nag, *ACS Energy Lett.* 2017, **2**, 1089.
74. X. Li, J. Yu, M. Jaroniec, and X. Chen, *Chem. Rev.* 2019, **119**, 3962.
75. J. Ran, M. Jaroniec, and S. Z. Qiao, *Adv. Mater*. 2018, **30**, 1704649.
76. Z. Zhang, A. Li, S. W. Cao, M. Bosman, S. Li, and C. Xue, *Nanoscale* 2014, **6**, 5217.
77. W. Gao, M. Wang, C. Ran, and L. Li, *Chem. Commun*. 2015, **51**, 1709.
78. J. Ran, J. Zhang, J. Yu, M. Jaroniec, and S. Z. Qiao, *Chem. Soc. Rev*. 2014, **43**, 7787.
79. A. Meng, J. Zhang, D. Xu, B. Cheng, and J. Yu, *Appl. Catal.. B* 2016, **198**, 286.
80. A. Meng, L. Zhang, B. Cheng, and J. Yu, *ACS Appl. Mater. Interfaces* 2018, **11,** 5581.
81. K. Maeda, K. Teramura, D. Lu, N. Saito, Y. Inoue, and K. Domen, *Angew. Chem., Int. Ed.* 2006, **45,** 7806.
82. Y. Shiraishi, H. Sakamoto, Y. Sugano, S. Ichikawa, and T. Hirai, *ACS Nano* 2013, **7**, 9287.
83. Z. Xiong, Z. Lei, C.-C. Kuang, X. Chen, B. Gong, Y. Zhao, J. Zhang, C. Zheng, and J. C. S. Wu, *Appl. Catal. B* 2017, **202**, 695.
84. S. Cao, Y. Chen, C. C. Hou, X. J. Lv, and W.F. Fu, *J. Mater. Chem. A* 2015, **3**, 6096.
85. M.B. Faheem, B. Khan, Y. Zhang, H. Li, M. Saud, H. Lin, H. Zhang, S.B. Ahmed, V. Vanshika, R. Qiao, and P. Kaswekar, *ACS Energy Letters*, 2025, **10**, 3337-3348.
86. J. Zhang, Y. Tang, K. Lee, and M. Ouyang, *Science* 2010, **327**, 1634−1638.

87. M. Liu, M. B. Johnston, and H. J. Snaith, *Nat. Commun.* 2013, **501**, 395−398.
88. D. Pan, Y. Fu, N. Spitha, Y. Zhao, C. R. Roy, D. J. Morrow, D. D. Kohler, J. C. Wright, and S. Jin, *Nat. Nanotechnol* 2021, **16**, 159−165.
89. Y. Zhao, M. Boccard, S. Liu, J. Becker, X. H. Zhao, C. M. Campbell, E. Suarez, M. B. Lassise, Z. Holman, and Y. H. Zhang, *Nat. Energy* 2016, **1**, 16067.
90. X. Li, W. Zhang, X. Guo, C. Lu, J. Wei, and J. Fang, *Science* 2022, **375**, 434−437.
91. M. Zhu, Z. Sun, M. Fujitsuka and T. Majima, *Angew. Chem., Int. Ed*. 2018, **57**, 2160−2164.
92. A. Tavasoli, A. Gouda, T. Zahringer, Y. F Li, H. Quaid, C. J. Viasus Perez, R. Song, M. Sain, and G. Ozin, *Nat. Commun*. 2023, **14,** 1435.
93. X. Li, C. Garlisi, Q. Guan, S. Anwer, K. Al-Ali, G. Palmisano, and L. Zheng, *Mater. Today* 2021, **47,** 75−107.
94. S. Mazzanti, S. Cao, K. Brummelhuis, A. Völkel, J. Khamrai, D. I. Sharapa, S. Youk, T. Heil, N. V. Tarakina, V. Strauss, I. Ghosh, B. König, M. Oschatz, M. Antonietti, and A. Savateev, *Appl. Catal., B* 2021, **285**, 119773.
95. A. Dey, J. Ye, A. De, E. Debroye, S. K. Ha, E. Bladt, A. S. Kshirsagar, Z. Wang, J. Yin, Y.Wang, L. N. Quan, F. Yan, M. Gao, X. Li, J. Shamsi, T. b. Debnath, M. Cao, M. A. Scheel, S. Kumar, J. A. Steele, M. Gerhard, L. Chouhan, K. Xu, X. Wu, Y. Li, Y. Zhang, A. Dutta, C.Han, I. Vincon, and A. L. Rogach., *ACS Nano* 2021, **15,** 10775.
96. J. S. Manser, J. A. Christians, and P. V. Kamat, *Chem. Rev.* 2016, **116**, 12956.
97. S. Chen, H. Yin, P. Liu, Y. Wang, and H. Zhao, *Adv. Mater*. 2023, **35**, 2203836.
98. A. Kojima, K. Teshima, Y. Shirai, and T. Miyasaka, *J. Am. Chem. Soc.* 2009, **131**, 6050.
99. A. Swarnkar, V. K. Ravi, and A. Nag, *ACS Energy Lett*. 2017, **2**, 1089.
100. Z. Xiao, Z. Song, and Y. Yan, *Adv. Mater*. 2019, **31**, 1803792.
101. H. Zhao, K. Kordas, and S. Ojala, *J. Mater. Chem*. A 2023, **11**, 22656.
102. J. Chen, C. Dong, H. Idriss, O. F. Mohammed, and O. M. Bakr, *Adv. Energy Mater*. 2019, **11**, 1004212.
103. S. Pan, J. Li, Z. Wen, R. Lu, Q. Zhang, H. Jin, L. Zhang, Y. Chen, and S. Wang, *Adv. Energy Mater.* 2022, **12**, 2004002.
104. M. Ahlawat, Neelakshi, R. Ramapanicker, and V. Govind Rao, *ACS Energy Lett*. 2023, **8**, 2159.
105. P. Cheng, K. Han, and J. Chen, *ACS Mater. Lett.* 2023, **5**, 60.
106. J. T. DuBose, and P. V. Kamat, *ACS Energy Lett*. 2022, **7**, 1994.
107. S. Park, W. J. Chang, C. W. Lee, S. Park, H.-Y. Ahn, and K. T. Nam, *Nat. Energy* 2016**,** **2**, 16185.108.
108 Q. Niu, W. Chen, G. Pan, L. Li, Y. Yu, J. Bi, L. Wu and J.C. Yu, 2024. *ACS Mater. Letters*, 2024, ***6***, 1411-1417.
109 P. Cheng, K. Han, and J. Chen, *ACS Mater. Letters*, 2022, **5,** 60-78.
110 C. Yan, Y. Qian, Z. Liao, Z. Le, Q. Fan, H. Zhu, and Z. Xie, *Photochem. & Photobio. Sciences*, 2024, **23**, 1393-1415.

111 M. Zhang, W. Sun, H. Lv, and Z.H. Zhang, *Current Opinion in Green and Sust. Chemistry*, 2021, **27**, 100390.
112. S. T. Ha, R. Su, J. Xing, Q. Zhang, and Q. Xiong, *Chem. Sci.* 2017**, 8**, 2522−2536.
113. T. M. Brenner, D. A. Egger, L. Kronik, G. Hodes, and D. Cahen, *Nat. Rev. Mater*. 2016, **1**, 15007.
114. E. Mosconi, A. Amat, M. K. Nazeeruddin, M. Grätzel, and F. De Angelis, J. *Phys. Chem. C* 2013, **117**, 13902−13913.
115. C. Wehrenfennig, G. E. Eperon, M. B. Johnston, H. J. Snaith, and L. M. Herz, *Adv. Mater*. 2014, **26**, 1584−1589.
116. Y. S. Kwon, J. Lim, H. J. Yun, Y. Kim, and T. A. Park, *Energy Environ. Sci.* 2014, **7**, 1454−1460.
117. J. A. Christians, P. A. Miranda Herrera, and P. V. Kamat, *J. Am. Chem. Soc.* 2015, **137**, 1530−1538.
118. J. Yang, B. D. Siempelkamp, D. Liu, and T. L. Kelly, *ACS Nano* 2015, **9,** 1955−1963.
119. G. Niu, X. Guo, and L. Wang, *J. Mater. Chem*. *A* 2015, **3**, 8970−8980.
120. J. B. Huang, S. Q. Tan, P. D. Lund, and H. P. Zhou, *Energy Environ. Sci*. 2017, **10**, 2284−2311.
121. C.L. Allen and J.M. Williams, *Chem. Soc. Reviews*, 2011, **40,** 3405-3415.
122. W. Wu, Y.C. Wong, Z. K. Tan, and J. Wu, *Catal. Sci. & Technol*., 2018, **8**, 4257-4263.
123. L. Xu, S. Z. Zhang, W. Li, and Z. H. Zhang, *Chem. Eur. J.,* 2021, **27**, 5483–5491.
124. L. Deng, L. Chen, L. Zhu, Y. Li, J. Ou-Yang, S. Wu, P. Chen, S. Shen, J. Guo, Y. Zhou, C. T. Au and S. F. Yin, *Chem. Eng. Sci.,* 2022, **261**, 117960.
125. B. Goel, V. Vyas, N. Tripathi, A. K. Singh, P. W. Menezes, A. Indra, and S.K. Jain, *ChemCatChem,* 2020, **12**, 5743-5749.
126. V. Vyas, V. Kumar and A. Indra, *Chem. Commun.,* 2024, **60**, 2544–2547.
127. O. G. Mountanea, D. Psathopoulou, C. Mantzourani, M. G. Kokotou, E. A. Routsi, D. Tzeli, C. G. Kokotos, and G. Kokotos, *Chem. Eur. J.* 2023, **29**, 2300556.
128. N. Martín and F. G. Cirujano, *Catal. Commun.,* 2022, **164,** 106420.
129. A. Hassan Tolba, M. Krupička, J. Chudoba and R. Cibulka, *Org. Lett.,* 2021, **23**, 6825–6830.
130. J. He, B. Han, C. Xian, Z. Hu, T. Fang, and Z. Zhang, *Angew. Chem. Int. Edt.,* 2024, **63**, 202404515.
131. F. Monnier and M. Taillefer, *Angew. Chem. Int. Ed.,* 2008, **47**, 3096–3099.
132. M. T. Pirnot, Y. Wang and S. L. Buchwald, *Angew. Chem. Int. Ed.,* 2016, **55**, 48–57.
133. M. R. Ball, T. S Wesley, K. R. Rivera-Dones, G. W. Huber, and J. A. Dumesic, *Green Chem.* 2018, **20**, 4695−4709
134. A. Corma, J. Navas and M. J. Sabater, *Chem. Rev..,* 2018, **118,** 1410–1459.
135. Z. Chi, J. Bin Liao, X. Cheng, Z. Ye, W. Yuan, Y. M. Lin, and L. Gong, *J. Am. Chem. Soc*., 2024, **146,** 10857–10867.
136. M. H. S. A. Hamid, C. L. Allen, G. W. Lamb, A. C. Maxwell, H. C. Maytum, A. J. A.

Watson, and J. M. J. Williams, *J. Am. Chem. Soc.,* 2009, **131**, 1766–1774.
137. G. Zou, R. Cao, C. Cui, Y. Luo, C. Huang, X. Cui, Z. Wang and Y. Song, *Catal. Sci. Technol.,* 2023, **13**, 3916–3926.
138. J. J. A. Celaje, X. Zhang, F. Zhang, L. Kam, J. R. Herron and T. J. Williams, *ACS Catal.,* 2017, **7**, 1136–1142.
139. H. Liu, D. L. Wang, X. Chen, Y. Lu, X. L. Zhao and Y. Liu, *Green Chem*., 2017, **19,** 1109–1116.
140. R. Kawahara, K. I. Fujita, and R. Yamaguchi, *J. Am. Chem. Soc.,* 2010, **132**, 15108–15111.
141 J. He, B. Han, C. Xian, Z. Hu, T. Fang, and Z. Zhang, *Angew. Chemi. Int. Edt.*, 2024, **63,** 202404515.
142 Y. Yuan, J. Wang, H. Liu and H. Li, 2023. *J. Mater. Chemistry A*, 2023, **11**, 24127-24135.
143. C. Huang, Y. Huang, C. Liu, Y. Yu, and B. Zhang, *Angew. Chem. Int. Ed*. 2019, **131**, 12142-12145.
144. R. Zhang, N. Chen, T. Ning, Y. Zhang, Y. Ling, X. Wang, W. Zhu and G. Zhu, *Inorg. Chem*. 2023, **62**, 17433–17443.
145. Z. Zhou, X. Pan, L. Sun, Y. Xie, J. Zheng, L. Li, and G. Zhao, *Angew. Chem. Int. Ed.* 2023, **62**, 202216347.
146. Z. Zhang, W. Liu, Y. Zhang, J. Bai, and J. Liu, *ACS Catal.* 2021, **11**, 313–322.
147. N. O. Balayeva, Z. Mamiyev, R. Dillert, N. Zheng, and D. W. Bahnemann, *ACS Catal.* 2020, **10,** 5542–5553.
148. S. Kato, Y. Saga, M. Kojima, H. Fuse, S. Matsunaga, A. Fukats. M. Kondo, S. Masaoka, and M. Kanai, *J. Am. Chem. Soc.* 2017, **139**, 2204–2207.
149 M. Zheng, J. Shi, T. Yuan, and X. Wang *Angew. Chem. Int. Ed.*. 2018, **57**, 5487–5491.
150 J. Luo, X. Wei, Y. Qiao, C. Wu, L. Li, L. Chen, and J. Shi *Adv. Mat.* 2023, **35**, 2210110.
151 M. Hao, X. Deng, L. Xu, and Z. Li, *Appl. Catal. B Environ.* 2019, **252**, 18–23.